# Orbital contribution to the magnetic properties of iron as a function of dimensionality

Marie-Catherine Desjonquères,[1] Cyrille Barreteau,[1] Gabriel Autès,[1] and Daniel Spanjaard[2]
[1]*CEA Saclay, DSM/DRECAM/SPCSI, Bâtiment 462, F-91191 Gif sur Yvette, France*
[2]*Laboratoire de Physique des Solides, Université Paris Sud, Bâtiment 510, F-91405 Orsay, France*
(Received 21 March 2007; revised manuscript received 27 April 2007; published 9 July 2007)

The orbital contribution to the magnetic properties of Fe in systems of decreasing dimensionality (bulk, surfaces, wire, and free clusters) is investigated using a tight-binding Hamiltonian in an *s*, *p*, and *d* atomic orbital basis set including spin-orbit coupling and intra-atomic electronic interactions in the full Hartree-Fock (HF) scheme, i.e., involving all the matrix elements of the Coulomb interaction with their exact orbital dependence. Spin and orbital magnetic moments and the magnetocrystalline anisotropy energy (MAE) are calculated for several orientations of the magnetization. The results are systematically compared with those of simplified Hamiltonians which give results close to those obtained from the local spin density approximation. The full HF decoupling leads to much larger orbital moments and MAE which can reach values as large as $1\mu_B$ and several tens of meV, respectively, in the monatomic wire at the equilibrium distance. The reliability of the results obtained by adding the so-called orbital polarization ansatz (OPA) to the simplified Hamiltonians is also discussed. It is found that when the spin magnetization is saturated, the OPA results for the orbital moment are in qualitative agreement with those of the full HF model. However, there are large discrepancies for the MAE, especially in clusters. Thus, the full HF scheme must be used to investigate the orbital magnetism and MAE of low dimensional systems.

DOI: 10.1103/PhysRevB.76.024412 PACS number(s): 75.75.+a, 75.30.Gw, 75.90.+w

## I. INTRODUCTION

The magnetic properties of reduced dimensionality systems are an area of growing interest both for experimentalists and theoreticians. Indeed, the spin magnetic moment of an atom is strongly dependent on its environment, in particular, on its coordination number. It usually increases when the latter decreases and may even appear in small clusters for some transition metals which are not magnetic in the bulk phase.[1–4] Another quantity playing a key role in technological applications, such as magnetic recording, is the magnetocrystalline anisotropy energy (MAE) which is responsible for the tendency of the magnetization to align along particular directions. It is well known that this MAE is very small in the bulk phase (some $\mu$eV) of ferromagnetic transition metals[5,6] but may increase by several orders of magnitude when the dimensionality or the symmetry of the system is reduced[7,8] (some meV for a free monolayer). The most striking specific property of low dimensional systems is perhaps the appearance of a sizable orbital contribution to the magnetic moment[9] which, on the contrary, is practically quenched in bulk systems. Obviously, the influence of intra-atomic Coulomb interactions and spin-orbit coupling, responsible for Hund's rules in the free atom, become more and more important when the bandwidth due to electron delocalization decreases and both the spin and orbital moments should tend to their atomic values. Furthermore, the interest for the orbital moment has been stimulated by a newly acquired physical technique, the x-ray magnetic circular dichroism (XMCD), which is able to resolve spin and orbital moments.[10] Such experiments have been carried out by Gambardella *et al.*[11,12] who have indeed measured orbital moments as large as $0.68\mu_B$ for Co chains on Pt(997) and $1.1\mu_B$ for a Co adatom on Pt(111), the corresponding MAE being 2 and 9 meV per Co atom, respectively. More recently, using the same technique, Lee has obtained an orbital moment of about $0.6\mu_B$ for Fe monatomic chains on Pt(997).[13] Moreover, XMCD experiments carried out on iron clusters[14,15] have shown that the orbital moment is much more enhanced than the spin moment as the size is reduced.

From the theoretical point of view, the spin moment can be obtained in the local spin density approximation (LSDA) or with a Stoner-like tight-binding (TB) Hamiltonian[16] but the spin orientation is arbitrary. This is not true when spin-orbit coupling is taken into account and, consequently, the MAE and the orbital moment no longer vanish. Pioneering works in which the spin-orbit coupling is treated as a perturbation have been carried out by Bruno[17] and Wang *et al.*,[7] for example. However, in these schemes the Hamiltonian depends only on the total spin density (LSDA) or spin population at each site (TB) and not on their repartition between the orbital states. In other words, electronic interactions are averaged, which yields underestimated values of MAE and orbital moments, even though these quantities increase when the dimensionality is reduced.[18,19] Eriksson *et al.*[20] have proposed to correct this drawback by adding to the total energy a term proportional to $-\frac{1}{2}\langle\mathbf{L}\rangle^2$ which will be referred to as the orbital polarization ansatz (OPA) in the following. This obviously tends to increase $\langle\mathbf{L}\rangle$ but is not really justified as we will see below.

A more rigorous way of obtaining the correct distribution of electrons between the *d* orbital states of opposite magnetic quantum numbers *m* is to take into account all intra-atomic terms in the Hartree-Fock (HF) decoupling of the two-body operators representing electron-electron interactions in the Hamiltonian with the exact expression of the matrix elements $U_{\gamma_1\gamma_2\gamma_3\gamma_4}$ of $e^2/|\mathbf{r}-\mathbf{r}'|$ as a function of the three Racah parameters *A*, *B*, and *C* relative to *d* atomic orbitals $\gamma_\alpha$.[6] Note that when using L(S)DA or a TB Hamiltonian parametrized by fits on L(S)DA calculations, some electronic inter-

 

actions are implicitly already included. This is usually accounted for by assuming that on each atom all spin-orbitals (all spin-orbitals with the same spin) are equally populated in LDA (LSDA).

Some attempts have been made in this direction. However, most often the terms involving three and four different orbitals have been neglected, which destroys the rotational invariance of the interaction Hamiltonian[21] unless appropriate averages of the matrix elements with two different orbitals are done.[22,23] Nevertheless, there exist in the literature some scarce calculations in which all matrix elements of the Coulomb interactions were taken into account[6,24,25] but, at least to our knowledge, no systematic study comparing this complete HF scheme to the OPA has been carried out save for our preliminary work on the Fe monatomic wire[26] in the TB approximation with an atomic orbital basis set restricted to *d* orbitals. Such a comparison is indeed very interesting since Solovyev *et al.*[27] have shown, in an elegant work, that the OPA cannot be derived analytically from the full HF Hamiltonian except in some very special cases. In the present work, we generalize our previous study,[26] on the one hand, by using a realistic description of the electronic states including *sp-d* hybridization in order to get quantitative results and, on the other hand, by investigating systems with various dimensionalities (bulk, surfaces, wire, clusters).

The paper is organized as follows. The formalism and the choice of parameters for Fe are described in Sec. II. Sections III and IV are devoted to bulk and surfaces of bcc iron, respectively. Our results concerning the monatomic wire and some clusters are given in Secs. V and VI. Finally, conclusions are drawn in Sec. VII.

## II. FORMALISM

The Hamiltonian of the system is written as

$$H = H_{TB} + H_{\mathrm{SO}} + \Delta H_{\mathrm{int}}, \tag{1}$$

where $H_{TB}$ is a tight-binding Hamiltonian parametrized for the nonmagnetic state by fitting *ab initio* calculations in the local density (LDA) or generalized gradient (GGA) approximation, $H_{\mathrm{SO}}$ is the spin-orbit coupling term, and $\Delta H_{\mathrm{int}}$ describes the change in electronic interactions with respect to $H_{TB}$.

We choose a nonorthogonal basis set made of the real *s*, *p*, and *d* valence atomic orbitals (i.e., cubic harmonics for reasons which will become clear in the following) centered at each site *i*. They are denoted by λ and $\mu$ indices $(\lambda,\mu=1,9)$ and numbered as follows: $s, p_x, p_y, p_z, d_{xy}, d_{yz}, d_{zx}, d_{x^2-y^2}, d_{3z^2-r^2}$ (the *x*, *y*, and *z* coordinates being taken along the crystal axes) with overlap integrals $S_{ij}^{\lambda\mu}$ depending on the bonding direction $\mathbf{R}_{ij}$. The Hamiltonian $H_{TB}$ is completely determined by its intra-atomic matrix elements (i.e., the *s*, *p*, and *d* atomic levels) $\epsilon_{i\lambda}$ and its interatomic matrix elements (i.e., the hopping integrals) $\beta_{ij}^{\lambda\mu}(\mathbf{R}_{ij})$. The functions $S_{ij}^{\lambda\mu}(\mathbf{R}_{ij})$ and $\beta_{ij}^{\lambda\mu}(\mathbf{R}_{ij})$ are given by the same analytical expressions as a function of two sets (one for overlap and one for hopping) of ten Slater-Koster (SK) integrals $(ss\sigma, sp\sigma, sd\sigma, pp\sigma, pp\pi, pd\sigma, pd\pi, dd\sigma, dd\pi, dd\delta)$ and of the direction cosines of $\mathbf{R}_{ij}$.[28] Following the scheme developed by Mehl and Papaconstantopoulos (MP),[29] the atomic levels depend on the atomic environment (number of neighbors and interatomic distances), while the SK integrals are functions of $R_{ij}$ only. The atomic levels and the SK integrals are written as analytic functions depending on a number of parameters which are determined by a least mean square fit of the results of *ab initio* LDA or GGA electronic structure (band structure and total energy) calculations. These parametrizations will be denoted respectively as TBLDA and TBGGA in the following: the analytical forms of the functions can be found in Ref. 29 and the numerical values of the parameters for Fe in Ref. 30.

The spin-orbit coupling Hamiltonian $H_{\mathrm{SO}}$ is given by

$$H_{\mathrm{SO}} = \xi \mathbf{L}\cdot\mathbf{S}, \tag{2}$$

where $\mathbf{L}$ and $\mathbf{S}$ are the orbital and spin momentum operators, respectively. Due to the local character of this interaction, only the intra-atomic matrix elements between *d* spin-orbitals have been taken into account. For more details, the reader is referred to Ref. 16 where $\xi$ has been determined ($\xi$=0.06 eV).

Only the intra-atomic electronic interactions are taken into account. For *d* electrons, they are written in the Hartree-Fock approximation, i.e.,

$$H_{\mathrm{int},dd}^{\mathrm{HF1}} = \sum_{\substack{i\gamma_1\gamma_2\gamma_3\gamma_4(3)\\ \sigma\sigma'}} (U_{\gamma_4\gamma_2\gamma_3\gamma_1}\langle n_{i\gamma_3\gamma_4}^{\sigma\sigma}\rangle c_{i\gamma_2\sigma'}^{\dagger} c_{i\gamma_1\sigma'} - U_{\gamma_4\gamma_2\gamma_1\gamma_3}\langle n_{i\gamma_3\gamma_4}^{\sigma'\sigma}\rangle c_{i\gamma_2\sigma'}^{\dagger} c_{i\gamma_1\sigma}), \tag{3}$$

as a function of the net density matrix $\langle n_{i\gamma_1\gamma_2}^{\sigma\sigma'}\rangle = \langle c_{i\gamma_2\sigma'}^{\dagger} c_{i\gamma_1\sigma}\rangle$ when all intra-atomic matrix elements of the Coulomb interactions, i.e.,

$$U_{\gamma_1\gamma_2\gamma_3\gamma_4} = \langle \gamma_1(\boldsymbol{r}), \gamma_2(\boldsymbol{r}')\left|\frac{e^2}{|\boldsymbol{r}-\boldsymbol{r}'|}\right|\gamma_3(\boldsymbol{r}), \gamma_4(\boldsymbol{r}')\rangle, \tag{4}$$

where $\gamma_i$ are a set of atomic *d* orbitals, are retained (HF1 model of Ref. 26). These matrix elements can be expressed as a function of the three Racah parameters *A*, *B*, and *C*.[31] This Hamiltonian is rotationally invariant in spatial as well as in spin coordinates since the spin-flip terms (i.e., with $\sigma' \neq \sigma$) arising from spin-orbit coupling are present in $H_{\mathrm{int},dd}^{\mathrm{HF1}}$.

Let us now comment on our choice for the basis set. Obviously, when all terms are present in $H_{\mathrm{int},dd}^{\mathrm{HF1}}$, the results do not depend on the basis set. This may not be the case when some matrix elements are omitted. For instance, in a common approximation, the terms involving three and four different orbitals are neglected.[22,32] When using a basis set made of spherical harmonics denoted by the value of the quantum number *m*, the three and four orbital terms are a function of both *B* and *C*. Therefore, if these terms are neglected without changing the one and two different orbital matrix elements, the rotational invariance is destroyed unless we set $B=C=0$, in which case the Coulomb-type integrals $U_{mm'mm'}=A$ are completely isotropic and the exchange integrals $U_{mm'm'm}$ vanish. This model is thus oversimplified if we want to study spin and orbital magnetism. On the con-

trary, when the basis set is built from cubic harmonics, the three and four orbital matrix elements are a function of $B$ only.[31] When these terms are neglected, the rotational invariance is conserved only if $B$ is set equal to zero. Then, in this model $U_{\lambda\mu\lambda\mu}=A+C$ and $U_{\lambda\mu\mu\lambda}=C$ for any pair $\lambda$, $\mu$ of different $d$ orbitals. This model can correctly describe spin magnetism by an appropriate choice of the parameters but cannot really account for orbital magnetism as shown in Ref. 26 on a simple model. This suggests redefining the parameters determining the HF1 Hamiltonian as $U$, $J$, $B$ with $U=(1/4)\Sigma_{\mu,\mu\neq\lambda}U_{\lambda\mu\lambda\mu}$ and $J=(1/4)\Sigma_{\mu,\mu\neq\lambda}U_{\lambda\mu\mu\lambda}$, the sums being independent of $\lambda$. These average values of Coulomb and exchange interactions are given by $U=A-B+C$ and $J=5B/2+C$. Thus, we expect that in the HF1 model the orbital magnetism, which is sensitive to the anisotropy of electronic interactions, is mainly governed by $B$ similar to what is assumed in the orbital polarization ansatz.

In the following, we will also consider the HF2 model of Ref. 26 which is obtained from HF1 by setting $B=0$ and sometimes called the $U,J$ model. Finally, a Stoner-like model called HF3 can be derived from HF1 under the following assumptions: (i) the net density matrix $\langle n_{i\lambda\mu}^{\sigma\sigma'}\rangle$ is diagonal with elements equal to the net occupation numbers $n_{i\lambda\sigma}$ and (ii) on each site $i$ the exact $n_{i\lambda\sigma}$ are replaced by their average value $n_{i\sigma}=1/5\Sigma_\lambda n_{i\lambda\sigma}$. Then, it is easily shown (see Appendix A) that the simplified Hamiltonian can be written as

$$H_{\mathrm{int},dd}^{\mathrm{HF3}}=\sum_{i\lambda\sigma}(U_{\mathrm{eff}}N_{i,d}-\sigma I_{dd}M_{i,d}/2)c_{i\lambda\sigma}^{\dagger}c_{i\lambda\sigma}, \tag{5}$$

where $U_{\mathrm{eff}}=(9U-2J)/10$, $I_{dd}=(U+6J)/5$ is the $d$ Stoner parameter, $N_{i,d}(M_{i,d})$ are the net $d$ total population (spin momentum) at site $i$, and $\sigma=+1(-1)$ for majority (minority) spin. Note that the above conditions are approximately obeyed for bulk transition metals but become questionable when the symmetry is lowered.

We must not forget that some electronic interactions are already included in $H_{TB}$ since this Hamiltonian has been parametrized by fitting LDA and GGA calculations. This is taken into account following the treatment done in the "around mean field" LDA+$U$ theory,[32] i.e.,

$$\Delta H_{\mathrm{int},dd}=H_{\mathrm{int},dd}(n_{i\lambda\mu}^{\sigma\sigma'})-H_{\mathrm{int},dd}(\bar{n}_i\delta_{\lambda\mu}\delta_{\sigma\sigma'}), \tag{6}$$

with $\bar{n}_i=\Sigma_{\lambda\sigma}n_{i\lambda\sigma}/10$, whatever the model (HF1, HF2, or HF3).

Finally, the small exchange splittings of the $s$ and $p$ levels due to the spin polarization of $d$ electrons are treated with a Stoner-like model and a Stoner parameter $I_{sd}=I_{pd}=I_{dd}/10$, i.e.,

$$\Delta H_{\mathrm{int},s(p)d}=-\sigma I_{s(p)d}M_{i,d}/2, \tag{7}$$

so that

$$\Delta H_{\mathrm{int}}=\Delta H_{\mathrm{int},sd}+\Delta H_{\mathrm{int},pd}+\Delta H_{\mathrm{int},dd}. \tag{8}$$

From the above discussion, it is clear that HF2 differs from HF1 by terms proportional to $B$; this is also true for HF3 as far as this Hamiltonian is justified. Eriksson *et al.*[20] have proposed to introduce an OPA term to account for this difference. This term is written in mean field $\Delta E_{\mathrm{OP}}=-\frac{1}{2}B\Sigma_i\langle \boldsymbol{L}_i\rangle^2$ which reduces to $-\frac{1}{2}B\Sigma_i\langle L_{iZ}\rangle^2$ when the spin and orbital moment $\langle \boldsymbol{L}_i\rangle$ are collinear with the axis $Z$ which is verified along high-symmetry directions (in the following, $X$, $Y$, $Z$ will denote the framework in which $Z$ is the spin magnetization direction). The corresponding Hamiltonian is then

$$H_{\mathrm{OP}}=-B\sum_{i\lambda\mu\sigma}\langle L_{iZ}\rangle[L_{iZ}]_{\lambda\mu}c_{i\lambda\sigma}^{\dagger}c_{i\mu\sigma}, \tag{9}$$

where $[L_{iZ}]_{\lambda\mu}$ are the matrix elements of the local-orbital moment operator $L_{iZ}$. Note that in the basis of cubic harmonics, $[L_{iZ}]_{\lambda\mu}$ is not diagonal.[16] In the following, we also compare the results obtained with HF1 to those derived from HF2 or HF3 to which the OPA term has been added.

As in our previous work,[16] we use the HF3 model to determine the Stoner parameter $I_{dd}$ so as to reproduce as closely as possible the variation of the bulk spin magnetic moment as a function of the interatomic distance that can be obtained from a spin polarized density-functional theory calculation. This gives $I_{dd}=1$ eV. Finally, from Fig. 1 of the recent work by Solovyev[33] it can be deduced that $U\simeq J$. As a consequence, we have taken $U=J=5I_{dd}/7=0.71$ eV and similar to most previous works $B=0.14J$.[33]

## III. SPIN AND ORBITAL MAGNETISM IN BULK BCC IRON

Let us first consider the bulk bcc phase of Fe and compare the results obtained with HF1 and HF3 using the TBGGA parameters. Indeed, we do not expect strong differences between HF2 and HF3 for the following reasons. First, in the absence of the small perturbation due to spin-orbit coupling, the intra-atomic density matrix is diagonal for symmetry reasons in cubic crystals. Second, the populations of the different orbitals with a given spin are rather similar in the bulk.

Calculations show that the equilibrium lattice parameter (5.35 a.u.) is close to the experimental value (5.43 a.u.) and that the variation of the spin moment with the lattice parameter is almost the same with the HF1 and HF3 models. For instance, the spin moments are $2.34\mu_B$ and $2.39\mu_B$ with HF1 and HF3, respectively (see Fig. 1) at the experimental equilibrium lattice parameter. On the opposite, the orbital moment is significantly enhanced with the HF1 model (see Fig. 2) and in very good agreement with experiment ($0.08-0.09\mu_B$) (Ref. 34) as well as with the theoretical results of Xie and Blackman.[6]

## IV. SPIN AND ORBITAL MAGNETISM AT BCC IRON SURFACES

We have applied the HF1 and HF3 models to the study of the (001) and (110) surfaces of bcc iron. The surfaces are modeled by slabs of 15 atomic layers which is sufficient to avoid interactions between the two surfaces and to recover the bulk behavior on the central layer. Interlayer relaxations are neglected in all calculations and the interatomic distance is set equal to the experimental one ($d_{\mathrm{bulk}}^{\mathrm{exp}}=4.69$ a.u.). In such systems, some atoms have a reduced coordination compared to the bulk and therefore charge transfers are expected. In

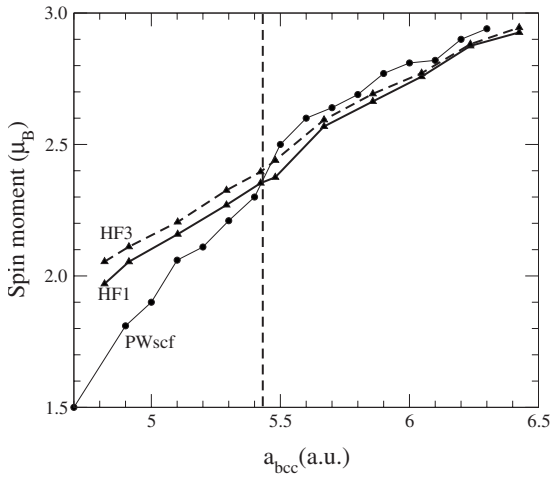


FIG. 1. Spin magnetic moment of bulk bcc iron as a function of the cubic lattice parameter from PWSCF *ab initio* calculations, HF1 and HF3 models. The dashed straight line corresponds to the experimental equilibrium lattice parameter.

order to avoid unphysically large charge transfers at the surface, we have used a penalty function (see Appendix B) which consists in adding to the energy functional a term of the type

$$E_{\mathrm{LCN}}^{\mathrm{pen}} = \lambda_{\mathrm{LCN}}^{\mathrm{pen}} \sum_i (\Delta q_i)^2. \tag{10}$$

Here, $\Delta q_i = q_i - q_0$, where $q_i$ is the Mulliken charge of site $i$ and $q_0$ the valence charge, and $\lambda_{\mathrm{LCN}}^{\mathrm{pen}}$ is the penalization factor which must be taken large enough to ensure local charge neutrality (in practice, one takes $\lambda_{\mathrm{LCN}}^{\mathrm{pen}} = 2.5$ eV which gives charge transfers below 0.1 electron per atom). The local charges $q_i$ are expressed as a function of the tight-binding expansion coefficients $C_{i\lambda\sigma}^n$ of the eigenfunctions $n$ with respect to the atomic orbitals,

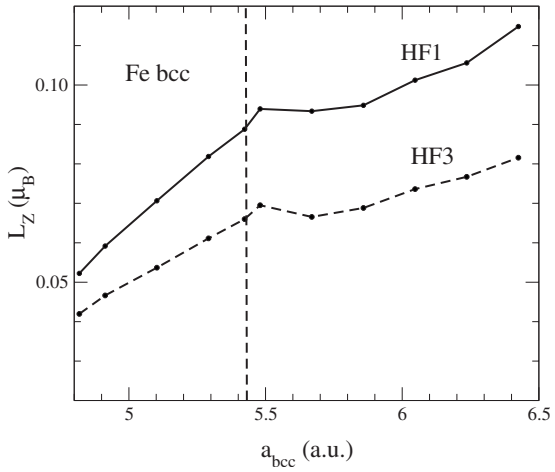


FIG. 2. Orbital magnetic moment of bulk bcc iron as a function of the cubic lattice parameter from the HF1 and HF3 models. The dashed straight line corresponds to the experimental equilibrium lattice parameter.

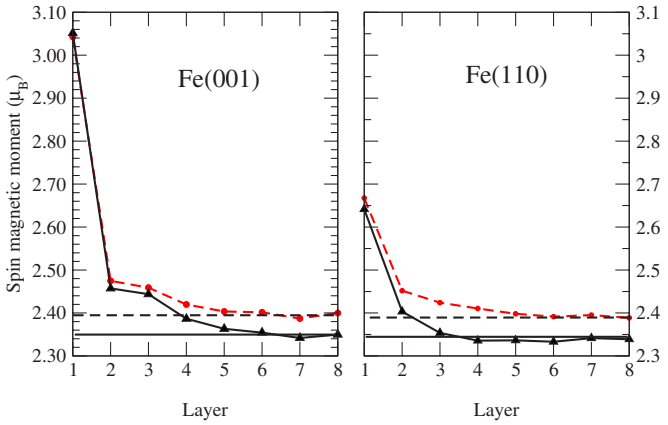


FIG. 3. (Color online) Variation of the spin magnetic moment (per atom) on successive layers of (001) and (110) slabs (with 15 atomic layers) of bcc Fe obtained from HF1 (full lines) and HF3 (dashed lines) models. Layer 1 corresponds to the outermost layer and layer 8 to the central layer. The horizontal lines correspond to the bulk limit.

$$q_i = \mathrm{Re}\left( \sum_{\substack{\lambda j \mu \sigma \\ n}} f_n C_{i\lambda\sigma}^{n\star} C_{j\mu\sigma}^{n} S_{ij}^{\lambda\mu} \right), \tag{11}$$

where $f_n$ is the occupation factor and depends on the type of system. In periodic systems such as surfaces, a broadening technique is used and $f_n = f(\varepsilon_n)$ is equal to the Fermi function at the energy level $\varepsilon_n$ for a given temperature.

A standard iterative scheme is set up until input and output intra-atomic density-matrix elements differ by less than $10^{-4}$ electron per atom and the total energy of the slab does not change by more than $10^{-4}$ eV. We have calculated the spin and orbital moments decomposed on each atomic layer of the (001) and (110) slabs. The results of our calculations are shown in Figs. 3 and 4. As expected, the spin magnetic moment is enhanced in the vicinity of the surface, this rein-

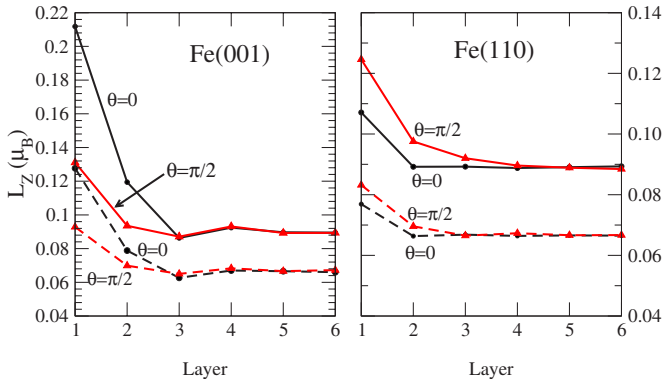


FIG. 4. (Color online) Variation of the component of the local-orbital magnetic moment on the magnetization direction as a function of the atomic layer in the (001) and (110) slabs (15 layers) for a magnetization perpendicular ($\theta = 0$) and parallel ($\theta = \pi/2$) to the surface from HF1 (full lines) and HF3 (dashed lines) models. For in-plane magnetization, the dependence of the orbital moment on the orientation in the plane is negligible.

forcement being more pronounced for the (001), for which the spin moment of the outermost layer is almost saturated, than for the (110) slab since the (001) surface is more open than the (110). The convergence to the bulk spin moment is also slightly faster for the (110) slab than for the (001) slab. Finally, apart from a small shift of the bulk spin moment between HF1 ($2.34\mu_B$) and HF3 ($2.39\mu_B$), the two models lead to very similar results. Let us also note that we have verified that the spin moment is almost independent of the magnetization orientation.

At surfaces, the orbital moment is also strongly enhanced. However, in contrast to the spin moment the type of model used is now crucial. Indeed, the enhancement of the orbital magnetization at the surface is much more pronounced with the HF1 model than with HF3. For magnetization perpendicular to the surface, one finds values of $\langle L_{iZ}\rangle$ as large as $0.21\mu_B$ on the outermost layer of the (001) surface with the HF1 model, while it is $0.127\mu_B$ with the HF3 model. Note that this latter value is in very good agreement with the results of Eriksson *et al.*[18] derived from LSDA calculations without OPA, i.e., $0.12\mu_B$ for a surface atom of a seven layer slab. The orbital moment is therefore 2.40 times larger at the surface than it is in the bulk ($0.088\mu_B$) with HF1, while it is slightly less than twice larger with HF3. The orbital polarization effect is therefore amplified at the surface: a 63% increase of the surface orbital moment between HF3 and HF1 is obtained, which must be compared to 33% in the bulk ($0.088\mu_B$ with HF1 and $0.066\mu_B$ with HF3). This general trend is also observed on the (110) surface though not so pronounced. Finally, contrary to the case of the spin moment the orbital moment $\langle L_{iZ}\rangle$ depends sensitively on the magnetization direction, and moreover the two surfaces behave differently. It is found that the orbital moment is noticeably larger for magnetization perpendicular to the surface in the case of the (100) slabs, while a slight increase of the orbital moment is observed for in-plane magnetization in the case of (110) slabs. In that respect, HF1 and HF3 models lead to very similar behaviors. Finally, one should point out that for in-plane magnetization the dependence of the orbital moment on the orientation in the plane is negligible.

## V. MAGNETIC PROPERTIES OF AN IRON MONATOMIC WIRE

In a preliminary work,[26] we already investigated the orbital contribution to the magnetic properties of the Fe monatomic wire and checked the ability of the OPA to account for the existence of large orbital moments in one-dimensional structures by comparing to the results obtained from a full Hartree-Fock decoupling of intra-atomic electronic interactions. To this aim, we used a simple tight-binding model in which only $d$ electrons were taken into account. However, in this model only the self-consistent solution(s) of the Hamiltonian could be determined but not the total energy. Furthermore, the number of $d$ electrons was fixed. On the contrary, the use of an $s$, $p$, $d$ basis set allows a charge redistribution between $sp$ and $d$ orbitals as a function of the interatomic distance $d$ and the determination of the total energy. In the following, we present the results obtained for a monatomic Fe wire with this realistic basis set using the TBLDA MP parameters for reasons which have been discussed in Ref. 16. This will enable us to confirm the qualitative trends obtained in the previous model and to get quantitative results.

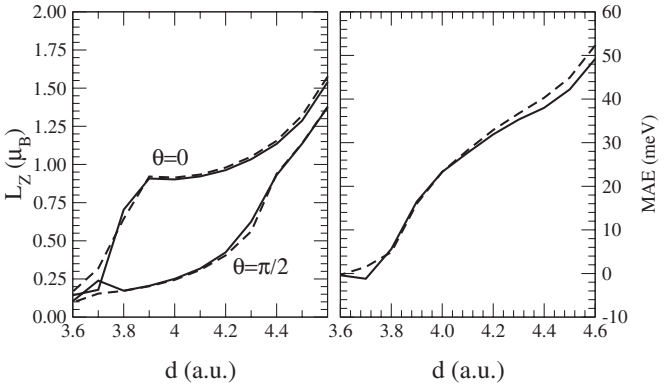


FIG. 5. Comparison between the results obtained with the HF2+OPA (full lines) and HF3+OPA (dashed lines) Hamiltonians for the monatomic Fe wire as a function of interatomic distance: (left) orbital moment for directions of magnetization parallel ($\theta=0$) and perpendicular ($\theta=\pi/2$) to the wire and (right) the corresponding magnetocrystalline anisotropy energy.

We have computed the total energy, the spin and orbital magnetic moments, the band structure, and the electronic transmission factor as a function of the interatomic distance for the different models, i.e., HF1 and HF2 or HF3 without and with OPA. The results show that the equilibrium distance is quite insensitive to the model chosen and is close to 4.05 a.u. (2.14 Å) with a slight dispersion smaller than 0.02 a.u. The spin magnetic moment is quite independent of the direction of magnetization. This moment is also almost unchanged when the OPA term is added to HF2 or HF3. Finally, the spin moment saturates between 3.7 and 3.8 a.u. for HF1 and HF2, and this saturation occurs at a shorter distance (between 3.6 and 3.7 a.u.) with HF3. Note that these latter results are in much better agreement with *ab initio* calculations [3.8 a.u. (Ref. 16)] than in the pure $d$-band model.

Let us now compare the orbital magnetic moments and MAE obtained with the various models. The models HF2 and HF3 with (Fig. 5) or without OPA give very similar results save for $3.6<d<3.8$ a.u., i.e., the domain of distances for which at least one of these models leads to an unsaturated spin moment. As a consequence, we will now limit ourselves to the comparison between the HF1, HF3, and HF3+OPA Hamiltonians for magnetizations parallel ($\theta=0$) and perpendicular ($\theta=\pi/2$) to the wire. A glance at Fig. 6 confirms, as expected, that HF3 largely underestimates the orbital moment $\langle L_Z\rangle$ for both magnetization directions and the MAE. Adding the OPA to HF3 obviously increases these quantities; however, for the orbital moment the difference with the result derived from HF1 does not keep the same sign as a function of the interatomic distance and is rather large in relative value when the spin is not saturated. Nevertheless, the overall agreement between HF1 and HF3+OPA is qualitatively satisfying. Note that if the OPA term were

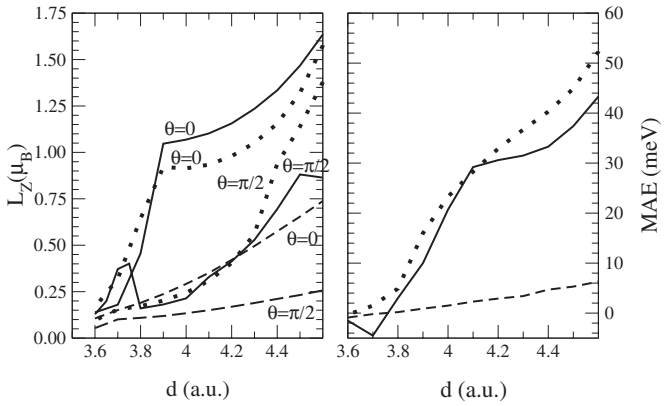


FIG. 6. Same as Fig. 5 but for the HF1 (full lines), HF3 (dashed lines), and HF3+OPA (dotted lines) Hamiltonians. Note that the curves referring to HF1 correspond to the most stable self-consistent solution for each value of $d$ (see text).

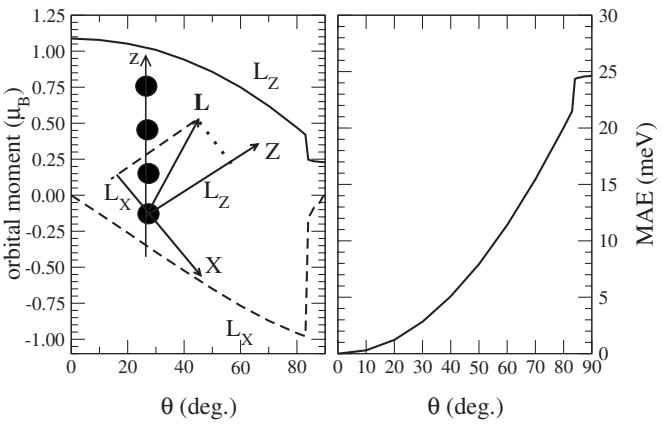


FIG. 7. Variation of the components of the orbital moment (left) and of the magnetic anisotropy energy (right) as a function of the direction of magnetization given by the angle $\theta$ for a monatomic wire (interatomic distance $d$=4.05 a.u.) obtained from HF1.

multiplied by 3 as suggested in a recent work by Narita and Higuchi[35] based on atomic structure calculations for the maximal spin multiplet, this agreement would be destroyed.

It is worthwhile to discuss the results given by HF1 in more detail. First, at $\theta$=0 a sharp change of slope occurs for $\langle L_Z\rangle$ at $d$=3.9 a.u. Let us recall[26] that at $\theta$=0 the wire eigenfunctions corresponding to the almost flat $\delta$ bands located near the Fermi level are a linear combination of $d$ spherical harmonics (with $m$=2 or $m$=−2) centered at each site. When $d$ increases from 3.6 a.u., the population of the highest energy band $m$=−2 decreases and vanishes for $d \simeq 3.9$ a.u. This explains the change of slope in the $\langle L_Z\rangle$ curve. Note also that for $d>4.3$ a.u., two self-consistent solutions are found corresponding to an empty band either with $m$=2 or $m$=−2 character and nearly opposite values of $\langle L_Z\rangle$. However, the solution in which the $m$=−2 band is empty and $\langle L_Z\rangle>0$ is always the most stable one. On the contrary, at $\theta=\pi/2$ the character of the eigenfunctions of the $\delta$ bands near the Fermi level is $d_{xy}$ or $d_{x^2-y^2}$. Up to $d$=4. a.u., these two bands are quasidegenerate. Then, when $d \geqslant 4.1$ a.u., two self-consistent solutions are found for which either $d_{xy}$ or $d_{x^2-y^2}$ are empty but, contrary to what occurs at $\theta$=0, they have almost the same total energy and very similar values of $\langle L_Z\rangle$. The change of slope at $d$=4.5 a.u. corresponds to the switch of the ground state from one case (empty $d_{x^2-y^2}$ band) to the other (empty $d_{xy}$ band). Finally, let us comment about the structure around $d$=3.7 a.u. As stated above, the spin moment saturates in this region, more precisely between $d$ =3.75 a.u. and $d$=3.76 a.u. and, around these values, two self-consistent solutions are also found: an unsaturated one with a rather large value of $\langle L_Z\rangle$ and a saturated one with a low value of $\langle L_Z\rangle$, which are the ground states for $d$ <3.75 a.u. and $d>3.76$ a.u., respectively.

It is interesting to compare our results with those of our previous works. The most striking result is perhaps the very high value that is reached by the MAE. This is in contrast with the case of Fe wires embedded in bulk Cu (Ref. 36) in which the MAE is only slightly enhanced compared to the case of bulk iron. This shows that the geometrical environment of the wire is crucial in determining its orbital magnetic properties, as also revealed in the work of Ederer *et al.*[37] for the orbital moment. In Ref. 16 we showed, using a Stoner-like Hamiltonian, that the proportionality relation between the MAE and the anisotropy of the orbital moment proposed by Bruno,[17] by treating the spin-orbit coupling by means of perturbation theory, is almost strictly verified when the interatomic distance in the wire is such that the spin moment is saturated. It is clear from Fig. 6 that this law is not satisfied with HF1 even though the MAE has the same sign as $\langle L_Z(\theta=0)\rangle - \langle L_Z(\theta=\pi/2)\rangle$.

To illustrate the departure from the perturbation theory, we have found useful to study the variation of the MAE and orbital magnetization with the angle between the monatomic wire and the magnetization axis. If one starts a calculation from a nonsymmetric magnetic configuration (different from $\theta$=0 or $\theta=\pi/2$) and let the self-consistent process iterate until convergency, it should bring the system toward the easy axis. Therefore, one has to find a way to follow the evolution with respect to the angle $\theta$. In order to constraint the angle $\theta$ between the spin moment and the $z$ axis, we add a penalty functional

$$E_{\text{ang}}^{\text{pen}} = \lambda_{\text{ang}}^{\text{pen}}(\cos\,\theta - \cos\,\theta_0)^2 \tag{12}$$

to the total energy (see Appendix B). In practice, $\lambda_{\text{ang}}^{\text{pen}}$ =1 eV ensures that the angle $\theta$ does not deviate by more than 0.1° from $\theta_0$. Figure 7 shows the results of our calculations with the HF1 model. This clearly shows that the orbital moment and the MAE are strongly modified when the anisotropy of the electronic interactions is taken into account. The MAE and the orbital moment no longer follow a simple $\sin^2\theta$ law and moreover present an abrupt variation around $\theta$=80° which corresponds to an electronic transition. Note that the position of this transition strongly depends on the interatomic distance. At larger interatomic distances, this transition occurs for smaller $\theta$ angles.

We must emphasize that the qualitative trends put forward in Ref. 26 are also obeyed when the basis set is extended to include $s$ and $p$ orbitals, namely, (i) the orbital moment and MAE are largely underestimated with a Stoner-like Hamil-

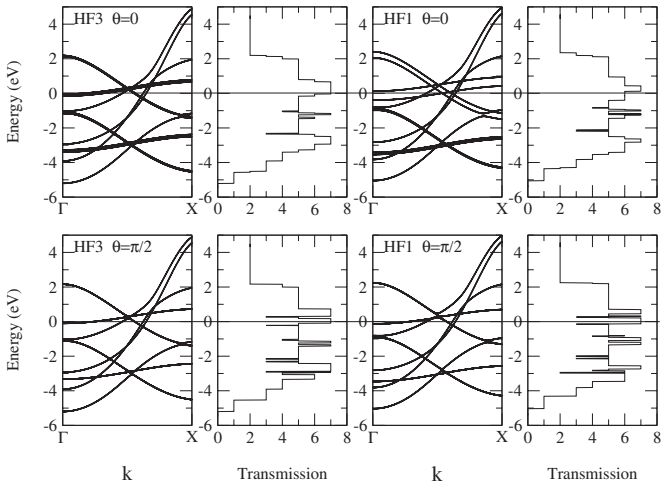


FIG. 8. Band structure and the corresponding electronic transmission factor of an iron monatomic wire for magnetizations parallel ($\theta=0$) and perpendicular ($\theta=\pi/2$) to the wire from the HF1 and HF3 models.

tonian but they reach numerical values similar to those observed experimentally in one-dimensional systems when HF1 is used, and (ii) adding the OPA to HF2 or HF3 leads to a fair agreement with HF1 for both $\langle L_Z \rangle$ and MAE when the spin moment is saturated but this agreement deteriorates in relative value for unsaturated spin polarization.

Finally, we show in Fig. 8 the band structure obtained with HF1 and HF3 for $\theta=0$ and $\theta=\pi/2$ at the equilibrium distance from which the electronic transmission factor $T(E)$ is deduced by a simple counting of the number of eigenfunctions at a given energy.[38] Some differences are observed, in particular, at $\theta=0$: around the Fermi level, the energy domain inside which $T(E)=7$ is narrowed when HF1 is used instead of HF3. Such differences should appear in more complex geometries such as those obtained in the constriction region of break junctions and could have important consequences on magnetoresistance properties.[39]

## VI. MAGNETIC PROPERTIES OF SOME IRON CLUSTERS

In the previous sections, we have studied three- (bulk), two- (surface), and one- (wire) dimensional periodic systems. To end this work, we have investigated zero-dimensional structures, i.e., unsupported clusters. We have considered five clusters with various geometries presented in Fig. 9.

Three of these clusters (triangle, square, and regular octahedron) are made of geometrically equivalent atoms, while the two others (cuboctahedron and icosahedron) are built from a central atom surrounded by 12 atoms forming the outer shell. Since it was shown in the previous section that HF2 and HF3 basically give the same results for saturated systems, we have restricted our study to the three models: HF1, HF3, and HF3+OPA. In a first step, we have minimized the total energy with respect to the nearest-neighbor distance. We only consider a homogeneous contraction of the

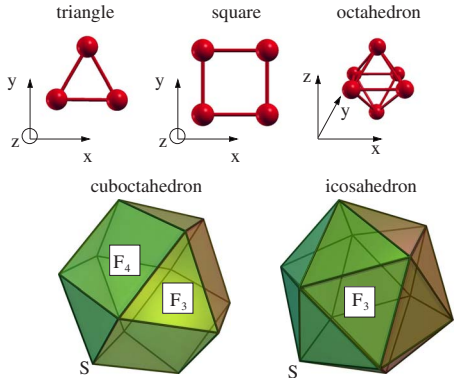


FIG. 9. (Color online) Geometry of the iron clusters. In the case of cuboctahedral and icosahedral geometries, each apex $S$ and the center of the cluster are occupied by an iron atom. $F_4$ and $F_3$ denote the center of a square and a triangular facet, respectively.

cluster and ignore Jahn-Teller distortions. Note that the discrete levels of the clusters have been filled with electrons up to the highest occupied molecular orbital (HOMO), i.e., the occupation factor $f_n=1$ or 0 except when the HOMO level is degenerate and not completely filled. In the latter case, the different wave functions corresponding to the HOMO level have been equally populated in order to preserve the cluster symmetry. Similar to the case of surfaces, a penalization function has been used to avoid large charge transfers (see Appendix B).

As illustrated in Fig. 10, the equilibrium interatomic distance is almost insensitive to the type of Hamiltonian. We also checked that the magnetization orientation does not influence the equilibrium distance either. As a consequence, the relaxed structures have been determined from HF3 calculations and a magnetization along a high-symmetry direction (see Fig. 9). The results are summarized in Table I. For all clusters, a contraction of the equilibrium bond length with respect to the calculated bulk one ($d_{\text{bulk}}=4.63$ a.u.) is obtained and the general trend stating that the contraction decreases with the average coordination is well obeyed. The interatomic distance of the triangle and square is contracted by 11%, the octahedron by 7%, and the cuboctahedron by

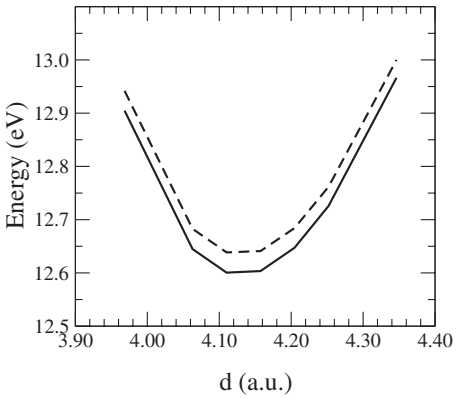


FIG. 10. Total energy as a function of the interatomic distance of a triangular iron cluster from HF1 (full line) and HF3 (dashed line) models. Note that the HF3+OPA curve would be undistinguishable from the HF3 one.

TABLE I. Equilibrium first nearest-neighbor distance of various iron clusters from HF3 calculations. Note that these values are almost identical to those obtained with HF1 calculations, and are almost independent of the magnetization axis. In the case of the icosahedron, $d_{eq}$ is the radial first nearest-neighbor distance $d_r$.

| | Triangle | Square | Octahedron | Cuboctahedron | Icosahedron |
|---|---|---|---|---|---|
| $d_{eq}$ (a.u.) | 4.14 | 4.16 | 4.31 | 4.50 | 4.42 |

3% with respect to the bulk. In the case of the icosahedron, one should distinguish between the radial $d_r$ and intrashell $d_t$ nearest-neighbor distance, the latter being about 5% larger than the former ($d_t=1.051d_r$). At equilibrium, one finds that the average value $(d_t+d_r)/2=4.53$ a.u. is very close to the interatomic distance of the cuboctahedron.

We have then carried out a detailed study of the MAE and of spin and orbital moments for these equilibrium structures with the three Hamiltonians. The spin moment is almost insensitive to the Hamiltonian used. We also found that the spin moment is carried by $d$ electrons and is almost saturated. Indeed, in spite of the contraction of interatomic distance relative to the bulk one which would tend to suppress magnetism, the strong decrease of coordination which favors spin polarization overcomes the first effect. Consequently, the $d$ spin moment $M_{i,d}$ on a given site $i$ can approximately be obtained from the number of $d$ electrons $N_{i,d}$ by the relation $M_{i,d}=10-N_{i,d}$. This simple rule is rather well obeyed for all clusters (see Table II) save for the cuboctahedron and icosahedron in which the central atom is depleted in $d$ electrons and is not saturated. Since it is well known from theoretical works that fcc iron has a tendency to form complicated magnetic structures, we have tried to start the self-consistent scheme for the cuboctahedron and icosahedron from an antiferromagnetic magnetic configuration. We were not able to find any antiferromagnetic solution except when allowing charge transfers by setting $\lambda_{\mathrm{LCN}}^{\mathrm{pen}}$ to zero. In that case, a rather large charge transfer is obtained (especially in the case of the icosahedron) from the inner atom to the outer shell, and one can find a self-consistent solution where the central atom has a spin magnetic moment opposite to that of outer-shell atoms. The ferromagnetic solution, however, remains the most stable solution.

Let us now discuss the MAE. First, it is worth noting that the MAE is quite sensitive to the interatomic distance. For illustration, we have calculated the MAE of a triangular iron cluster (see Fig. 11) as a function of the interatomic distance. As expected, the HF3 model systematically leads to smaller MAE than the HF1 or HF3+OPA model. Moreover, the MAE may change sign when the interatomic distance increases as seen in Fig. 11 where the easy axis switches from out of plane (positive MAE) to in plane (negative MAE) at $d=4.06$ a.u. with the HF3 model. It is also found that the in-plane anisotropy is extremely small and of the order of some hundredths of meV. The results are given in Table III for the five clusters at equilibrium. The behavior of the square cluster is very different from the triangular one since the three models agree to find an out-of-plane easy axis and a strong in-plane anisotropy (the diagonal axis being strongly unfavorable), but the numerical values are very dependent on the model (see Table III). The octahedron is the only cluster for which the three models agree to predict an absence of anisotropy (smaller than $2\times10^{-5}$ eV). Finally, the comparison of the cuboctahedron and icosahedron is instructive since these two structures only differ by small atomic displacements.[40] The cuboctahedron shows a rather large anisotropy in favor of the direction denoted as $F_3$, while the icosahedron shows a very weak anisotropy due to its more spherical shape. For both structures, the addition of the OPA term to HF3 does not lead to a significant improvement compared to HF1.

Since noncollinear magnetism is always a possible issue in clusters, we have checked for the five clusters that the most stable spin configuration is the ferromagnetic collinear one. To this aim, we have initialized our calculation by arbitrary noncollinear magnetic configurations and iterated until convergency. In most cases, a ferromagnetic collinear configuration is obtained. However, depending on the initial conditions, several collinear and noncollinear antiferromagneticlike configurations, (i.e., with zero total magnetic moment) are sometimes found, but their energy is always above the ferromagnetic one. Interestingly, when the calculation converges toward the ferromagnetic configuration, the self-consistent scheme proceeds as follows: in the first iterations, the magnetic moments tend to align along a given direction (depending on the initial condition), then once the moments are almost aligned, it takes a long time for the system to

TABLE II. Number of $d$ electrons $N_{i,d}$, $d$, and total spin moments $M_{i,d}$ and $M_i$ (in $\mu_B$) on each site of the five clusters. Note that these quantities are almost independent of the model, for instance, the spin moments do not differ by more than 0.01 $\mu_B$. The two values for the cuboctahedral and icosahedral clusters refer to the central and peripheral atoms, respectively.

| | Triangle | Square | Octahedron | Cuboctahedron | Icosahedron |
|---|---|---|---|---|---|
| $N_{i,d}$ | 7.21 | 7.24 | 7.31 | 6.80/7.14 | 6.90/7.12 |
| $M_{i,d}$ | 2.68 | 2.57 | 2.44 | 2.42/2.63 | 2.28/2.63 |
| $10-N_{i,d}$ | 2.79 | 2.76 | 2.69 | 3.20/2.86 | 3.10/2.88 |
| $M_i$ | 2.66 | 2.50 | 2.33 | 2.47/2.62 | 2.33/2.63 |

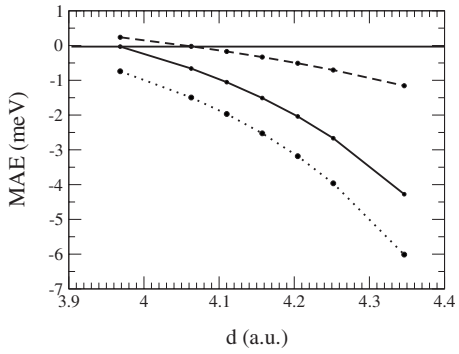


FIG. 11. Magnetic anisotropy energy (MAE) $E_{100}-E_{001}$ as a function of the interatomic distance of a triangular iron cluster from HF1 (full line), HF3 (dashed line), and HF3+OPA (dotted line) models. Note that the MAE curve $E_{010}-E_{001}$ would be undistinguishable from $E_{100}-E_{001}$ since there is almost no in-plane anisotropy.

converge toward the easy axis. For all clusters, we were able to find the easy axis by this procedure except for the cuboctahedron. In fact, in the latter case, depending on the initial conditions the calculation sometimes converges toward the $S$ (apex) configuration, sometimes toward the $F_3$ (center of triangular facet), meaning that the total energy possesses several local minima.

Let us now consider the orbital moment. The results of our calculations are presented in Tables IV and V. It is seen that the orbital moment is very sensitive to the magnetization orientation as at surfaces and in the monatomic wire. Furthermore, two structurally equivalent atoms now become "magnetically" inequivalent and can bear orbital moments that differ by a factor of more than 2. For instance, in a cuboctahedron with a magnetization pointing toward the center of the square facet $F_4$, the eight atoms forming the upper and lower square facets (with respect to the magnetization axis) have an orbital moment about twice smaller than that of the four other outer-shell atoms whatever the model. The orbital moment of the central atom is close to the bulk bcc value. In contrast, the icosahedron shows a more equally distributed orbital moment and the orbital moment on the central atom is significantly larger than in the bulk. Moreover, the difference between the values obtained from the various Hamiltonians is much less pronounced.

Finally, as expected and contrary to the spin moment, the type of Hamiltonian has most often a strong influence on the numerical value of the orbital moment. We find that HF3 systematically predicts the smallest ones. However, contrary to the case of MAE, there is now a fairly good agreement between HF1 and HF3+OPA. It should be pointed out that when two magnetic orientations have almost the same energy, the total orbital moments in these two directions are almost identical. This can be verified from Tables III and IV in the case of the (100) and (010) directions of the triangle. One should, however, not conclude that in the HF1 model the MAE is simply related to the orbital moment. Indeed, with this model, the easy axis of the triangle corresponds to the highest orbital moment but this is not true for the square.

TABLE III. Magnetic anisotropy energy in meV for various iron clusters from HF1, HF3, and HF3+OPA models calculated at the equilibrium interatomic distance. For the cuboctahedron and the icosahedron, the direction $\boldsymbol{u}$ is determined by the vector joining the central atom to an apex ($S$) and to the centers of a triangular facet ($F_3$) or a square facet ($F_4$).

| | Triangle | |
|---|---|---|
| | MAE=$E_{\boldsymbol{u}}-E_{001}$ (meV) | |
| $\boldsymbol{u}\rightarrow$ | (100) | (010) |
| HF1 | −1.264 | −1.270 |
| HF3 | −0.246 | −0.246 |
| HF3+OPA | −2.225 | −2.253 |
| | **Square** | |
| | MAE=$E_{\boldsymbol{u}}-E_{001}$ (meV) | |
| $\boldsymbol{u}\rightarrow$ | (100) | (110) |
| HF1 | 8.911 | 15.245 |
| HF3 | 5.378 | 6.3190 |
| HF3+OPA | 20.560 | 26.346 |
| | **Octahedron** | |
| | MAE=$E_{\boldsymbol{u}}-E_{001}$ (meV) | |
| $\boldsymbol{u}\rightarrow$ | (100) | |
| HF1 | −0.004 | |
| HF3 | −0.001 | |
| HF3+OPA | 0.021 | |
| | **Cuboctahedron** | |
| | MAE=$E_{\boldsymbol{u}}-E_{F_4}$ (meV) | |
| $\boldsymbol{u}\rightarrow$ | $S$ | $F_3$ |
| HF1 | −1.676 | −2.208 |
| HF3 | −0.331 | −0.441 |
| HF3+OPA | −0.358 | −0.359 |
| | **Icosahedron** | |
| | MAE=$E_{\boldsymbol{u}}-E_S$ (meV) | |
| $\boldsymbol{u}\rightarrow$ | $F_3$ | |
| HF1 | 0.114 | |
| HF3 | 0.020 | |
| HF3+OPA | −0.020 | |

## VII. CONCLUSION

In conclusion, this work presents an extended study of orbital polarization effects on the magnetic properties of iron systems with various dimensionalities using an $s,p,d$, tight-binding Hamiltonian with spin-orbit coupling and $dd$ intra-atomic electronic interactions treated in the Hartree-Fock scheme at different levels of approximations. The results obtained from the full Hartree-Fock interaction Hamiltonian HF1, i.e., involving all matrix elements of the Coulomb interactions with their exact orbital dependence as a function of the three Racah parameters, have been systematically compared with those of simplified Hamiltonians including or

TABLE IV. Local-orbital moments of iron triangular, square, and octahedral clusters for various spin magnetization orientations $Z$ (see Fig. 9), from HF1, HF3, and HF3+OPA Hamiltonians at the equilibrium distance. The number of sites having the same orbital moment for symmetry reasons is given in parentheses. In the case of the (110) direction of the square, the largest value corresponds to the diagonal of the square perpendicular to the magnetization.

| | Triangle | | |
|---|---|---|---|
| | | $\langle L_Z \rangle$ ($\mu_B$) | |
| **Z**→ | (001) | (100) | (010) |
| HF1 | 0.133 (3) | 0.177 (2) | 0.216 (2) |
| | | 0.236 (1) | 0.159 (1) |
| HF3 | 0.090 (3) | 0.112 (2) | 0.129 (2) |
| | | 0.138 (1) | 0.104 (1) |
| HF3+OPA | 0.130 (3) | 0.189 (2) | 0.229 (2) |
| | | 0.238 (1) | 0.159 (1) |
| | Square | | |
| | | $\langle L_Z \rangle$ ($\mu_B$) | |
| **Z**→ | (001) | (100) | (110) |
| HF1 | 0.325 (4) | 0.337 (4) | 0.234 (2) |
| | | | 0.259 (2) |
| HF3 | 0.255 (4) | 0.164 (4) | 0.133 (2) |
| | | | 0.142 (2) |
| HF3+OPA | 0.487 (4) | 0.362 (4) | 0.249 (2) |
| | | | 0.270 (2) |
| | Octahedron | | |
| | | $\langle L_Z \rangle$ ($\mu_B$) | |
| **Z**→ | (001) | (100) | |
| HF1 | 0.124 (4) | 0.128 (4) | |
| | 0.133 (2) | 0.124 (2) | |
| HF3 | 0.087 (4) | 0.094 (4) | |
| | 0.101 (2) | 0.087 (2) | |
| HF3+OPA | 0.128 (4) | 0.140 (4) | |
| | 0.153 (2) | 0.128 (2) | |

TABLE V. Local-orbital moments of iron for cuboctahedral and icosahedral clusters for various spin magnetization orientations $Z$ determined by the vector joining the central atom to an apex ($S$) and the centers of a triangular facet ($F_3$) or of a square facet ($F_4$), from HF1, HF3, and HF3+OPA Hamiltonians at the equilibrium interatomic distance. The number of sites having the same orbital moment for symmetry reasons is given in parentheses, except for the direction denoted as $F_3$ for which the orbital moments are very similar on all the external atoms. In the case of the $S$ direction of the cuboctahedron, the smallest orbital moment in the outershell corresponds to the two atoms with a binding direction parallel to the magnetization.

| | Cuboctahedron | | |
|---|---|---|---|
| | | $\langle L_Z \rangle$ ($\mu_B$) | |
| **Z**→ | $F_4$ | $S$ | $F_3$ |
| HF1 | 0.098 (1) | 0.101 (1) | 0.102 (1) |
| | 0.156 (8) | 0.246 (8) | ≈0.23 (12) |
| | 0.304 (4) | 0.153 (2) | |
| | | 0.182 (2) | |
| HF3 | 0.063 (1) | 0.063 (1) | 0.064 (1) |
| | 0.098 (8) | 0.143 (8) | ≈0.13 (12) |
| | 0.182 (4) | 0.095 (2) | |
| | | 0.104 (2) | |
| HF3+OPA | 0.103 (1) | 0.105 (1) | 0.105 (1) |
| | 0.158 (8) | 0.255 (8) | ≈0.23 (12) |
| | 0.321 (4) | 0.162 (2) | |
| | | 0.179 (2) | |
| | Icosahedron | | |
| | | $\langle L_Z \rangle$ ($\mu_B$) | |
| **Z**→ | $S$ | $F_3$ | |
| HF1 | 0.202 (1) | 0.202 (1) | |
| | 0.317 (10) | ≈0.32 (12) | |
| | 0.304 (2) | | |
| HF3 | 0.207 (1) | 0.207 (1) | |
| | 0.222 (10) | ≈0.22 (12) | |
| | 0.210 (2) | | |
| HF3+OPA | 0.271 (1) | 0.271 (1) | |
| | 0.312 (10) | ≈0.28 (6) | |
| | 0.268 (2) | ≈0.32 (6) | |

not the orbital polarization ansatz (OPA). Indeed, in usual approximations, the matrix elements of the Coulomb interaction are averaged. This may be a rather poor approximation when the orbitals are not equally populated since, for instance, the exchange matrix elements $U_{\lambda\mu\mu\lambda}$ may differ by factor of 2 depending on the considered orbital pair.[31] As expected, it is found that the one-parameter Stoner-like Hamiltonian HF3 which, similar to the L(S)DA approach, neglects the orbital dependence of Coulomb interactions leads to reasonable values of the spin moment but largely underestimates the orbital moment and the magnetocrystalline anisotropy energy (MAE). The two-parameter $(U,J)$ HF2 model, in which three and four orbital matrix elements are neglected and those with two different orbitals are averaged in the cubic harmonics basis, leads practically to the same results as the Stoner-like Hamiltonian, at least when the spin moment is saturated. In both these simplified Hamiltonians, the addition of the OPA, which is not really justified on theoretical grounds, gives largely improved values of the orbital moment but is much less reliable for the MAE, at least in clusters or when the spin moment is not saturated. With the full interaction Hamiltonian HF1, the orbital moment and the MAE attain numerical values of the same order of magnitude as those measured experimentally on supported clusters or chains,[11–13] although larger. This is not surprising since it is expected and confirmed by *ab initio* LSDA calculations including an OPA term[37] that a free monatomic chain has an orbital moment around twice as large as when supported with the same interatomic distance.

Furthermore, HF1 is fully rotationally invariant as well in spatial and in spin coordinates. The influence of spin-flip

terms is rather weak in the case of iron but is expected to increase drastically with the spin-orbit coupling parameter. This could be important for platinum which has been shown to be magnetic in monatomic wires.[41] Finally, it should be emphasized that it is not much more computer demanding to deal with the HF1 model. It is thus of prime importance to work with this model for the study of orbital magnetism and MAE in low dimensional systems either in a realistic *s*, *p*, *d*, tight-binding basis set or to implement it in *ab initio* codes of the LDA+$U$ type.

## APPENDIX A: RELATION BETWEEN HF1 AND HF3 INTERACTION HAMILTONIANS

In this appendix, we show, using the real *d* orbital basis set, that the Stoner-like Hamiltonian HF3 can be obtained from the full Hartree-Fock interaction Hamiltonian $H_{\mathrm{int},dd}^{\mathrm{HF1}}$ with the following approximations:

(i) The intra-atomic matrix density is assumed to be diagonal with respect to both orbital and spin indices.

(ii) For each spin and at each site, the exact population of the $\nu\sigma$ spin-orbital is replaced by its average value, i.e., $n_{i\sigma}=1/5\Sigma_{\nu}n_{i\nu\sigma}$, then the matrix elements of the approximate electronic interaction Hamiltonian become

$$H_{i\lambda\sigma,i\mu\sigma}=n_{i\sigma}\sum_{\nu}(U_{\nu\lambda\nu\mu}-U_{\nu\lambda\mu\nu})+n_{i-\sigma}\sum_{\nu}U_{\nu\lambda\nu\mu}. \quad \text{(A1)}$$

It can be shown[31] that the matrix elements $U_{\lambda\mu\nu\eta}$ vanish when three indices are equal and that the elements involving three different orbitals obey the relations $\Sigma_{\nu}U_{\nu\lambda\nu\mu}=0$ and $\Sigma_{\nu}U_{\nu\lambda\mu\nu}=0$. Consequently, the approximate Hamiltonian is diagonal and

$$H_{i\lambda\sigma,i\lambda\sigma}=n_{i\sigma}\sum_{\nu}(U_{\nu\lambda\nu\lambda}-U_{\nu\lambda\lambda\nu})+n_{i-\sigma}\sum_{\nu}U_{\nu\lambda\nu\lambda}. \quad \text{(A2)}$$

By replacing $n_{i\sigma}$ by $(N_{i,d}+\sigma M_{i,d})/10$, we find

$$H_{i\lambda\sigma,i\lambda\sigma}=\sum_{\nu}\left(U_{\nu\lambda\nu\lambda}-\frac{U_{\nu\lambda\lambda\nu}}{2}\right)\frac{N_{i,d}}{5}-\sigma\sum_{\nu}U_{\nu\lambda\lambda\nu}\frac{M_{i,d}}{10}. \quad \text{(A3)}$$

Carrying out the summations over $\nu$ leads to

$$H_{i\lambda\sigma,i\lambda\sigma}=\frac{9U-2J}{10}N_{i,d}-\frac{\sigma}{2}\left(\frac{U+6J}{5}\right)M_{i,d}, \quad \text{(A4)}$$

which are the matrix elements of the electronic interaction Hamiltonian in the HF3 model.

## APPENDIX B: PENALTY FUNCTIONS

The usual way to implement constraints in a variational problem is to use a Lagrange-multiplier formalism. For example, the normalization constraint of the wave functions leads to the eigenvalue problem, the Lagrange multiplier being the eigenvalues. However, this approach is not always very well suited to more general constraints. A very useful approach is to add a supplementary term to the total-energy function.[42,43] This term called penalty function is equal to zero when the constraint is fulfilled and large and positive when it is not. In the present work, we have used a local charge neutrality (LCN) penalty $E_{\mathrm{LCN}}^{\mathrm{pen}}$ and a $\theta$ angle penalty $E_{\mathrm{ang}}^{\mathrm{pen}}$. We have taken the following forms for these penalty functions:

$$E_{\mathrm{LCN}}^{\mathrm{pen}}=\lambda_{\mathrm{LCN}}^{\mathrm{pen}}\sum_{i}(\Delta q_i)^2 \quad \text{(B1)}$$

and

$$E_{\mathrm{ang}}^{\mathrm{pen}}=\lambda_{\mathrm{ang}}^{\mathrm{pen}}\sum_{i}(\cos\theta_i-\cos\theta_{i0})^2. \quad \text{(B2)}$$

Here, $\Delta q_i=q_i-q_0$, where $q_i$ is the Mulliken charge of site $i$ and $q_0$ the valence charge, $\lambda_{\mathrm{LCN}}^{\mathrm{pen}}$ ($\lambda_{\mathrm{ang}}^{\mathrm{pen}}$) is the penalization factor which must be taken large enough to ensure local charge neutrality (fixed angle), $\theta_i$ is the local spin magnetization angle on atom $i$, and $\theta_{i0}$ is the angle that one wants to impose. Using the expression of $q_i$ and $\cos\theta_i=M_{iz}/\sqrt{M_{ix}^2+M_{iy}^2+M_{iz}^2}$ in terms of the tight-binding expansion coefficients of the wave functions, the calculation of the derivative of the penalized total energy with respect to these expansion coefficients leads to an eigenvalue problem where the Hamiltonian is now modified by an additional "renormalizing" term which matrix elements reads

$$\lambda_{\mathrm{LCN}}^{\mathrm{pen}}(\Delta q_i+\Delta q_j)\sigma_0 S_{ij}^{\lambda\mu}$$

and

$$-\lambda_{\mathrm{ang}}^{\mathrm{pen}}(\boldsymbol{B}_i^{\mathrm{pen}}+\boldsymbol{B}_j^{\mathrm{pen}})\cdot\boldsymbol{\sigma}S_{ij}^{\lambda\mu},$$

in the case of LCN and angle penalization, respectively, where $\sigma_0$ is the identity matrix and $\boldsymbol{\sigma}$ the Pauli matrix vectors. $\boldsymbol{B}_i^{\mathrm{pen}}$ is an effective constraining magnetic field that exerts a torque to bring the magnetization along the $\theta_{i0}$ axis which expression is

$$\boldsymbol{B}_i^{\mathrm{pen}}=\lambda_{\mathrm{ang}}^{\mathrm{pen}}\frac{(\cos\theta_i-\cos\theta_{i0})}{(M_{ix}^2+M_{iy}^2+M_{iz}^2)^{3/2}}\begin{pmatrix}M_{ix}M_{iz}\\ M_{iy}M_{iz}\\ -M_{ix}^2-M_{iy}^2\end{pmatrix}. \quad \text{(B3)}$$

In practice, $\lambda_{\mathrm{LCN}}^{\mathrm{pen}}=2.5$ eV and $\lambda_{\mathrm{ang}}^{\mathrm{pen}}=1$ eV ensure charge transfers below 0.1 electron per atom and deviations from the angle $\theta_{i0}$ smaller than 0.1°.

The modified eigenvalue problem has to be solved iteratively until convergence of the Mulliken charges (and total energy). Finally, it should be noted that if one writes the total energy as a sum of the occupied eigenvalues, one should not forget to subtract an additional double-counting term arising from the penalization function.

[1] A. J. Cox, J. G. Louderback, S. E. Apsel, and L. A. Bloomfield, Phys. Rev. B **49**, 12295 (1994).
[2] R. Guirado-López, D. Spanjaard, and M. C. Desjonquères, Phys. Rev. B **57**, 6305 (1998).
[3] R. Guirado-López, D. Spanjaard, M. C. Desjonquères, and A. M. Oles, Eur. Phys. J. B **3**, 437 (1998).
[4] C. Barreteau, R. Guirado-López, D. Spanjaard, M. C. Desjonquères, and A. M. Oleś, Phys. Rev. B **61**, 7781 (2000).
[5] G. H. O. Daalderop, P. J. Kelly, and M. F. H. Schuurmans, Phys. Rev. B **41**, 11919 (1990), and references therein.
[6] Yuannan Xie and John A. Blackman, Phys. Rev. B **69**, 172407 (2004).
[7] Ding-sheng Wang, Ruqian Wu, and A. J. Freeman, Phys. Rev. B **47**, 14932 (1993).
[8] A. Lessard, T. H. Moos, and W. Hübner, Phys. Rev. B **56**, 2594 (1997).
[9] M. Tischer, O. Hjortstam, D. Arvanitis, J. H. Dunn, F. May, K. Baberschke, J. Trygg, J. M. Wills, B. Johansson, and O. Eriksson, Phys. Rev. Lett. **75**, 1602 (1995).
[10] H. Jaffrès, D. Bertrand, A. R. Fert, J. Vogel, A. Fontaine, N. B. Brookes, A. Schuhl, and F. N. Van Dau, Phys. Rev. B **63**, 174411 (2001).
[11] P. Gambardella, A. Dallmeyer, K. Maiti, M. C. Malagoli, W. Eberhardt, K. Kern, and C. Carbone, Nature (London) **416**, 301 (2002).
[12] P. Gambardella, S. Rusponi, M. Veronese, S. S. Dhesi, C. Grazioli, A. Dallmeyer, I. Cabria, R. Zeller, P. H. Dederichs, K. Kern, C. Carbone, and H. Brune, Science **300**, 1130 (2003).
[13] Tae-Yon Lee, Ph.D. thesis, Ecole Polytechnique Fédérale de Lausanne, 2005.
[14] K. W. Edmonds, C. Binns, S. H. Baker, M. J. Maher, S. C. Thornton, O. Tjernberg, and N. B. Brookes, J. Magn. Magn. Mater. **200**, 25 (2000).
[15] C. Binns, S. H. Baker, M. J. Maher, S. C. Thornton, S. Louch, S. S. Dhesi, and N. B. Brookes, Eur. Phys. J. D **16**, 189 (2001).
[16] G. Autès, C. Barreteau, D. Spanjaard, and M. C. Desjonquères, J. Phys.: Condens. Matter **18**, 6785 (2006).
[17] P. Bruno, Phys. Rev. B **39**, 865 (1989).
[18] Olle Eriksson, G. W. Fernando, R. C. Albers, and A. M. Boring, Solid State Commun. **78**, 801 (1991).
[19] Yuannan Xie and John A. Blackman, J. Phys.: Condens. Matter **16**, 3163 (2004).
[20] O. Eriksson, M. S. S. Brooks, and B. Johansson, Phys. Rev. B **41**, 9087 (1990).
[21] G. Nicolas, J. Dorantes-Davilá, and G. M. Pastor, Comput. Mater. Sci. **35**, 292 (2006).
[22] V. I. Anisimov, I. V. Solovyev, M. A. Korotin, M. T. Czyzyk, and G. A. Sawatzky, Phys. Rev. B **48**, 16929 (1993).
[23] M. Wierzbowska, A. Delin, and E. Tosatti, Phys. Rev. B **72**, 035439 (2005).
[24] A. I. Liechtenstein, V. I. Anisimov, and J. Zaanen, Phys. Rev. B **52**, R5467 (1995).
[25] A. B. Shick, F. Máca, and P. M. Oppeneer, Phys. Rev. B **69**, 212410 (2004).
[26] M. C. Desjonquères, C. Barreteau, G. Autès, and D. Spanjaard, Eur. Phys. J. B **55**, 23 (2007).
[27] I. V. Solovyev, A. I. Liechtenstein, and K. Terakura, Phys. Rev. Lett. **80**, 5758 (1998).
[28] J. C. Slater and G. F. Koster, Phys. Rev. **94**, 1498 (1954).
[29] M. J. Mehl and D. A. Papaconstantopoulos, Phys. Rev. B **54**, 4519 (1996).
[30] http://cst-www.nrl.navy.mil/bind/
[31] J. S. Griffith, *The Theory of Transition Metal Ions* (Cambridge University Press, London, 1961).
[32] M. T. Czyzyk and G. A. Sawatzky, Phys. Rev. B **49**, 14211 (1994).
[33] I. V. Solovyev, Phys. Rev. Lett. **95**, 267205 (2005).
[34] D. Bonnenberg, K. A. Hempel, and H. P. J. Wijn, *Magnetic Properties of Metals, Alloys, and Metallic Compounds*, Landolt-Börnstein, New Series, Group III, Vol. 19, Pt. A, edited by H. P. J. Wijn (Springer, Berlin, 1986).
[35] Akira Narita and Masahiko Higuchi, J. Phys. Soc. Jpn. **75**, 024301 (2006).
[36] Markus Eisenbach, Balazs L. Györffy, G. M. Stocks, and Balazs Újfalussy, Phys. Rev. B **65**, 144424 (2002).
[37] Claude Ederer, Matej Komelj, and Manfred Fähnle, Phys. Rev. B **68**, 052402 (2003).
[38] S. Datta, *Electronic Transport in Mesoscopic Systems* (Cambridge University Press, New York, 1995).
[39] M. Viret, M. Gabureac, F. Ott, C. Fermon, C. Barreteau, G. Autès, and R. Guirado-López, Eur. Phys. J. B **51**, 1 (2006).
[40] C. Barreteau, M. C. Desjonquères, and D. Spanjaard, Eur. Phys. J. D **11**, 395 (2000).
[41] A. Delin and E. Tosatti, Surf. Sci. **566-568**, 262 (2004).
[42] R. Gebauer, Ph.D. thesis, Ecole Normale Supérieure de Lyon, 1999.
[43] R. E. Cohen and S. Mukherjee, Phys. Earth Planet. Inter. **143-144**, 445 (2004).